Available online at www.sciencedirect.com

ScienceDirect

Solar Energy 132 (2016) 332–344

SOLAR ENERGY

www.elsevier.com/locate/solener

Validation of models that estimate the clear sky global and beam solar irradiance

Pierre Ineichen

University of Geneva, Energy System Group, F.A Forel Institute, Institute of Environmental Sciences, Switzerland

Received 8 April 2015; received in revised form 15 February 2016; accepted 8 March 2016

Communicated by: Associate Editor David Renne

Abstract

The optimal utilization of solar energy requires a thorough characterization of the solar resource. The most accurate way is to measure that resource in situ. However accurate measurements are not a common commodity, especially over longer time spans. To circumvent the lack of ground based measurements, models can be applied to estimate solar irradiance components. A fundamental component is clear sky irradiance. In particular, clear sky irradiance is used as the normalization function in models that convert meteorological satellite images into irradiance, or in models that decompose global irradiance into diffuse/direct fraction. It is therefore important to evaluate and validate clear sky irradiance models.

This paper presents the results of a validation of hourly clear sky models spanning up to eight years. The validation relies on high quality measurements at 22 locations in Europe and around the Mediterranean region. Seven models are evaluated. They were selected on the basis of their published performance, their simplicity of use, and/or their computational speed; two different sources of the aerosol load are used as input to the models.

The three best models show a low bias and a standard deviation ranging from ±3% to ±5%. The standard deviation of the bias across the 22 locations is of the same order of magnitude. The observed bias patterns can be largely traced to inaccuracies inherent to the sources aerosol optical depth. No particular seasonal effects are noted. A consistent limitation across all selected models, even if their direct irradiance performance can be judged satisfactory based on the standard deviation metric, is that they tend to fall short of observations for a given clear sky global clearness index value.

Keywords: Clear sky solar irradiance; Model validation; Daily aerosol optical depth; Water vapor column

1. Introduction

Anthropogenic activities have become an important factor in climate change. One of the aspects of this activity is an impact on the solar irradiance reaching the ground over the long term. It is essential to understand the impact of such changes on the environment (Cutforth, 2007; Stanhill, 2001). Unfortunately, the number and geographic distribution of quality ground irradiance measurement stations is insufficient to accurately access the global impacts of changes to solar irradiance at the surface, especially for direct normal (beam) irradiance (*DNI*). To circumvent this lack of ground measured data, meteorological satellites can be of great help. Models converting the satellite images into different radiation components such as SolarGIS (Suri, 2004; Cebecauer, 2011), EnMetSol (Hammer, 2009), Helioclim (Blanc, 2011), IrSOLaV (Zarzalejo, 2009), Solemi (Meyer, 2003), CM-SAF (Müller, 2009) or Heliomont

E-mail address: pierre.ineichen@unige.ch

http://dx.doi.org/10.1016/j.solener.2016.03.017
0038-092X/

Nomenclature

Solar radiation

GHI or G_h	horizontal global irradiance
DIF or D_h	horizontal diffuse irradiance
DNI or B_n	normal (beam) irradiance
B_h	horizontal beam irradiance
I_o	sun-earth distance corrected solar constant
K_t	global irradiance clearness index
K_t'	modified global clearness index
K_b	beam clearness index

Solar geometry

AM	optical air mass
z	solar zenith angle

Meteorologic measurements

T_a	ground ambient temperature
RH	relative humidity

Atmospheric parameters

α	size Angström coefficient
β	turbidity Angström coefficient
aod	aerosol optical depth
Δ_{cda}	clear and dry panchromatic optical depth
Δ_a	aerosol panchromatic optical depth
Δ_w	water vapor panchromatic optical depth
O_3	atmospheric ozone
T_{LAM2}	Linke turbidity coefficient at air mass 2
w	atmospheric water vapor content (or column)

Statistics

mbd	mean bias difference
sd	standard deviation
bsd	standard deviation of the bias

(Stoekli, 2013), are becoming increasingly efficient. The clear sky index (global irradiance normalized by the corresponding clear sky irradiance) is often effectively used in lieu of the clearness index (global irradiance normalized by the corresponding extra-atmospheric irradiance) to eliminate seasonal effects on stationary time series (Hansen, 2010), to derive typical meteorological years (TMY) from long term time series, or for forecasting purposes (Pelland, 2013; Engerer, 2014). The capability of these models to estimate the radiation reaching the ground is directly related to the precision of the clear sky model used as normalization function.

When the geographic and geometrical parameters are known (altitude, albedo, solar zenith angle, etc.), the two main input variables of clear sky models are the atmospheric aerosol optical depth (*aod*) and the total water vapor column (*w*). Whereas parameters like the total atmospheric amount of ozone or the NO_2 have a minor impact on solar radiation transmissivity, aerosol optical depth and water vapor have a substantial influence on the absorptivity and transmissivity of the radiation during its atmosphere crossing. Therefore, to obtain good estimates of the clear sky irradiance, these two inputs must be known with the best possible precision and a good time and space granularity. The atmospheric water vapor content (*w*) can be retrieved with relatively low uncertainty (±15%) from ground temperature (T_a) and relative humidity (*RH*) measurements (Smith, 1966; Atwater, 1976). Because of its higher spatial and temporal variability, accurate estimates of aerosol optical depth (*aod*) are based on photometric measurements. Unfortunately, measurements of *aod* are scarce, especially over the long term, and their spatial repartition is poor. It is therefore important to understand how the choice of a model and of its input data, influence the uncertainties of modeled clear sky irradiance.

In a previous study (Ineichen, 2006), the author presented a short-term (one-year) validation of clear sky models using Linke turbidity (Linke, 1922) climatic data banks as an input – Linke turbidity was converted to aerosol optical depth with the help of Ineichen model (Ineichen, 2002). In the present paper, a long term validation (up to eight years) of seven clear sky models is presented. This validation is based on daily aerosol atmospheric content derived from two sources: (1) ground measurements and (2) the MACC-II project (Kaiser et al., 2012).

2. Clear sky models

Seven of the best-performing and/or widely used models are selected for evaluation. The choice of models is based on their performance, their ease of use and their computation speed. These models require aerosol optical depth (*aod*) and water vapor column (*w*) as an input. Two of the models use Linke turbidity coefficient at air mass *2* (TL_{AM2}) as an input.

2.1. McClear model

The McClear is the most recent clear sky model. It is a fully physical model developed by Mines Paris Tech (Lefèvre, 2013). The core of the model consists of look-up tables (LUT) calculated with the help of the LibRadTran radiative transfer model (Mayer and Killing, 2005; Mayer et al., 2010) in a 10-dimensions space including aerosol optical depths at two wavelengths, partial aerosol optical depths for the determination of the aerosol type,

the water vapor column and the ozone amount. The model also uses the parameters derived from the MACC-II project.

2.2. Simplified Solis model

The original Solis model is a spectral clear sky model developed in the frame of the Heliosat-3 project (Mueller et al., 2004). It is also based on LibRadTran calculations in a 10-dimensions space including aerosol optical depths at two wavelengths, partial aerosol optical depths for the determination of the aerosol type, the water vapor column and the ozone amount. For application to satellite models, because the large spatial coverage, clear sky calculations should be fast, which is not the case when using LibRadTran. To increase computational speed, a broadband simplified version of Solis was derived by Ineichen (2008a,b). Look-up tables were calculated with LibRadTran for possible ranges of the input parameters, and least-square regressions were then applied to the data from the look-up tables. The second version (2008b) of the model includes rural, urban, maritime and tropospheric aerosol types (Shettle, 1989). The model requires panchromatic aerosol optical depth (at 700 nm) and water vapor column as inputs. The model is accurate and computationally fast.

2.3. CPCR2 model

CPCR2 is a physical model, parametrized in two solar spectrum bands – UV + visible and infrared. In each band a radiation modeling technique is applied and a transmittance of each extinction layer is parametrized to derive transmission functions for the beam and the diffuse components of the clear sky solar irradiance. The main input parameters to the model are the two Angström coefficients (the exponent (α) or the size parameter, and the turbidity coefficient (β)), and the water vapor column (w). The two Angström coefficients are related to the aerosol optical depth *aod* by the Angström relation. Average values for the single scattering albedo are used to differentiate types of aerosols. A complete description is given in Gueymard (1989).

2.4. REST2 model

The first version of REST, developed by Gueymard (2003) was limited to the beam component of the clear sky irradiance. REST2 is the two-bands version of the REST model, it uses the general features of CPCR2 with updated transmittance functions calculated with the SMARTS spectral model (Gueymard, 2001) and using the latest extraterrestrial spectral distribution and solar constant value. As for CPCR2, the main input parameters to the model are the water vapor column, the Angström turbidity coefficient (β) and aerosol size parameter (α). Average values for the single scattering albedo are used to differentiate between types of aerosols. A complete description is given in Gueymard (2004). Default values of 0.0002 atm-cm are applied for the reduced NO_2 scattering, and 340 Dobson units for the O3 vertical path length. REST2 and CPCR2 are the most flexible models in terms of input specificity.

2.5. Bird model

Bird and Hulström (1980) developed a transmittance expression for the different attenuation processes in the atmosphere and based on Radiative Transfer Model (RTM) calculation with SOLTRAN (RTM scheme constructed from LOWTRAN). The description can be found in Bird (1980). The model requires three input parameters: the water vapor column (in cm), the broadband aerosol optical depth (at 700 nm or calculated from the spectral attenuation at two wavelengths commonly used by meteorological networks: 380 and 500 nm), and the total ozone column considered here as constant and equal to 340 Dobson units. The model is simple to implement and widely used in the solar energy community.

2.6. ESRA model

The ESRA clear sky model was developed in the frame of the European Solar Radiation Atlas (ESRA, 2000) and used in the Heliosat-2 satellite model (Rigollier, 2000; Geiger, 2002). Contrary to other models, it derives separately the beam and the diffuse components that are added to obtain the global irradiance. The beam component is based on Kasten's (1996) Rayleigh optical depth parametrization and on the Linke turbidity at air mass 2. The clear sky diffuse irradiance is expressed as the product of a zenith diffuse transmission and a diffuse angular function.

2.7. Kasten model

The basis of the Kasten model is the pyrheliometric formula described in a paper from Kasten (1980). The irradiances are calculated by taking into account the absorption and scattering at two different altitude levels: 2500 m and 8000 m (Kasten, 1984). The model uses the Linke turbidity coefficient at air mass 2 to parametrize the aerosol load of the atmosphere. The atmospheric water vapor column is included in the Linke turbidity factor. Because the ESRA and the Kasten models are based on Linke turbidity, they are included in the study for comparison purposes.

3. Ground measurements

Hourly data from 22 measurement sites are used for model validation, with up to eight years of continuous measurements. Their geographic repartition is shown in Fig. 1. The sites' latitude, longitude, altitude and climate characteristics are reported in Table 1 along with the types of measurements available and the institute in charge of these measurements. Except for Skukuza, two or three

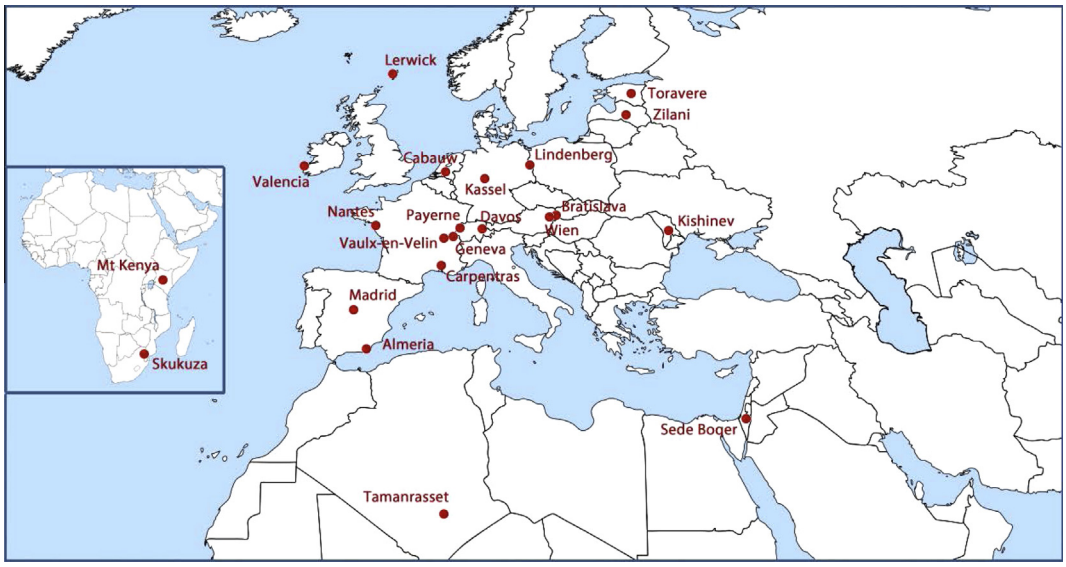

Fig. 1. Map of the ground measurement stations.

Table 1
List of the ground sites with the latitude, longitude, altitude, climate, the acquired parameters and the origin of the data.

Site	*GHI*	*DNI*	*DIF*		Lat	Long	Altitude	Climate	Data source
Almeria (Spain)	x	x	x	2004–2011	37.092	−2.364	491	dry, hot summer	PSA
Bratislava (Slovakia)	x		x	2004–2007	48.166	17.083	195	semi-continental	CIE
Cabauw (the Netherlands)	x	x	x	2005–2013	51.970	4.930	70	temperate maritim	BSRN
Camborne (Great Britain)	x	x	x	2004–2013	50.220	−5.310	88	oceanic	GAW
Carpentras (France)	x	x	x	2004–2013	44.083	5.059	100	mediternean	BSRN
Davos (Switzerland)	x	x	x	2004–2011	46.813	9.844	1586	alpine	PMO/SLF
Geneva (Switzerland)	x	x		2004–2013	46.199	6.131	420	semi-continental	CIE
Kassel (Germany)	x	x	x	2004–2011	51.312	9.478	173	temperate humide	FhG
Mt Kenya (Kenya)	x		x	2004–2007	−0.062	37.297	3678	warm humid	GAW
Kishinev (Moldavia)	x	x	x	2004–2013	47.000	28.817	205	continental humid	GAW
Lerwick (Great Britain)	x	x	x	2004–2013	60.133	−1.183	82	cold oceanic	GAW
Lindenberg (Germany)	x	x	x	2004–2010	52.210	14.122	125	moderate maritim	BSRN
Madrid (Spain)	x	x	x	2004–2011	40.450	−3.730	650	semi-arid	UMP
Nantes (France)	x		x	2004–2010	47.254	−1.553	30	oceanic	CSTB
Payerne (Switzerland)	x	x	x	2004–2011	46.815	6.944	490	semi-continental	BSRN
Sede Boqer (Israel)	x	x	x	2004–2012	30.905	34.782	457	dry steppe	BSRN
Skukuza (South Africa)	x			2006–2007	−25.020	31.497	365	steppe, hot arid	CSIR
Tamanrasset (Algeria)	x	x	x	2004–2011	22.780	5.510	1400	hot, desert	BSRN
Toravere (Estonia)	x	x	x	2004–2013	58.254	26.462	70	cold humid	BSRN
Valentia (Ireland)	x		x	2004–2013	51.938	−10.248	14	oceanic	GAW
Vaulx-en-Velin (France)	x	x	x	2004–2013	45.778	4.923	170	semi-continental	ENTPE
Wien (Austria)	x		x	2004–2013	48.250	16.367	203	continental	GAW
Zilani (Letonia)	x	x	x	2004–2009	56.520	25.920	107	cold humid	GAW

irradiance components are available. High precision instruments (WMO, 2008) such as Kipp and Zonen CM10 and Eppley PSP pyranometers, and Eppley NIP pyrheliometers, are used at each station. Following WMO recommendations, the instruments should be secondary standard pyranometers and pyrheliometers, their respective uncertainty for hourly values should not be higher than ±2% and ±1.5%. Taking into account the demanding maintenance of the sensors, it is estimated that the resulting data uncertainty under the worst conditions of maintenance can reach twice the WMO recommendation values. Stringent calibration, characterization and quality control (BSRN, 2015; Ineichen, 2014) have been applied to all data at each site. In addition, the coherence between the different irradiance components was checked by the author: the redundancy between the three global, diffuse and beam components is verified, and, if only two of them are available, a visual control is applied.

4. Input parameters

The two main parameters needed to calculate clear sky irradiance are the atmospheric aerosol optical depth (*aod*) and the water vapor column (*w*). The water vapor column

can easily be estimated from the ground measurements of the temperature (T_a) and the relative humidity (RH) with a ±15% uncertainty which induces a less than ±2% uncertainty on the evaluated clear sky irradiance. However it is not the case for the atmospheric aerosol content which requires specific data sources. In the present study, *aod* and w are evaluated in the following manner:

- When ground measurements of the ambient temperature and the relative humidity (or dew point temperature) are available, an approximation of the atmospheric water vapor content is obtained from correlations derived by Smith (1966) and adapted by Atwater (1976). When no ground measurements are available, monthly averages from Meteonorm or Helioclim are used (Meteonorm, 2009; Blanc, 2011);
- The atmospheric aerosol content can be obtained either (1) from the MACC-II project that *monitors the global distributions and long-range transport of greenhouse gases such has carbon dioxide and methane, aerosols that result from both natural processes and human activities, and reactive gases such as tropospheric ozone and nitrogen dioxide* (www.copernicus.eu), (2) from spectral measurements with Cimel instruments through the Aeronet network (Aeronet), or (3) by retrofit of the direct normal (beam) irradiance (DNI) with the help of Molineaux-Ineichen *bmpi* model described below. When the Linke turbidity factor is needed as input for a model, it is derived from *aod* using the conversion function developed by Ineichen (2002, 2008c).

From the station list, only three sites are part of the Aerosol Robotic Network (Aeronet): Cabauw, Carpentras and Toravere, and two of them are situated at high latitudes. To circumvent the lack of aerosol optical depth ground measurements, measured irradiance data are used to estimate a daily aerosol optical depth by applying a retrofit on the normal beam irradiance *DNI*. This is done with a model developed by Molineaux (1998) and referenced as the *bmpi* model:

Based upon numerically integrated spectral simulations from Modtran (Berk, 1996), Molineaux derived the following expression for the panchromatic (broad-band) optical depth of a clean and dry atmosphere with no aerosol loading:

$$\Delta_{cda} = -0.101 + 0.235 * AM^{-0.16}$$

He also produced the following expression for the panchromatic water vapor optical depth:

$$\Delta_w = 0.112 * AM^{-0.55} * w^{0.34}$$

where w is the precipitable water vapor content of the atmosphere in cm and AM the air mass. The precision of these fitted expressions is better than 1% when compared to Modtran simulations in the range $1 < AM < 6$ and $0 < w < 5$ cm. The following equation may then be applied to estimate the broad band aerosol attenuation Δ_a:

$$DNI = I_o \exp(-AM * (\Delta_{cda} + \Delta_w + \Delta_a))$$

where I_o is the sun-earth distance corrected solar constant.

To retrofit *aod* from *DNI* observations, the model is applied in the following way: when the atmospheric water vapor column w is known, the hourly profile of *DNI* is calculated for each day and for the complete range of considered *aod*. Then, the daily profile with the lowest quadratic difference with the measurements is kept; it is related to the best fit of the daily *aod* value.

The effectiveness of the retrofitting method is illustrated in Fig. 2 where the retrofitted *aod* is plotted versus the aeronet retrieved *aod* for the three locations where the latter is available. The mean slope is +5% away from the 1:1 diagonal, with a standard deviation of ±0.03 in optical depth units. The correlation coefficient is equal to 0.92.

The resulting impact of the retrofit method's precision on clear sky model validation is estimated to be of the order of ±1% for bias and less than ±0.5% for the standard deviation. It is therefore acceptable to apply the retrofit method to obtain daily *aod* when well calibrated and characterized *DNI* measurements are available. The precision of derived daily *aod* is sufficient to have only a marginal influence on the validity of the present clear sky model evaluation study. Moreover, all tested models are treated equal in this respect.

5. Clear sky models characteristics

In order to define physical limits for the measurements, the behavior of the models and the coherence between irradiance components are analyzed. To visualize these characteristics, model trends are represented for four typical values of aerosols optical depths (0.05, 0.1, 0.2 and 0.5) and a range of water vapor column; a value of $w = 1$ cm is kept for the illustrations. The ozone amount is taken constant at a value of 340 Dobson units, the aerosol characteristics is of rural type, with an Angström size coefficient $\alpha = 1.3$, and the albedo coefficient at 15%. Fig. 3 illustrates the Solis model, for 1 cm of water vapor column and rural aerosol type. The global clearness index K_t ($K_t = GHI/I_o$

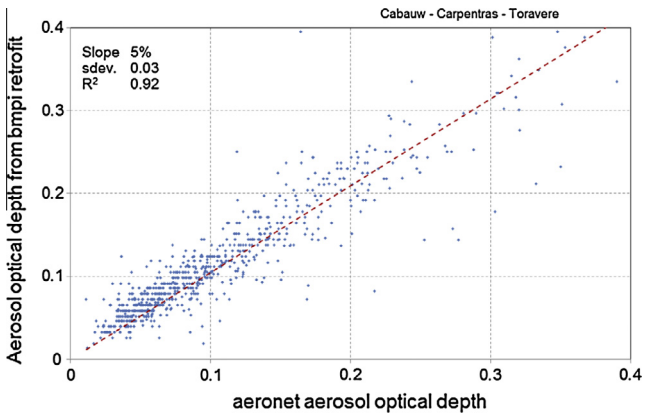

Fig. 2. Retrofitted *aod* versus aeronet *aod* for the 3 sites.

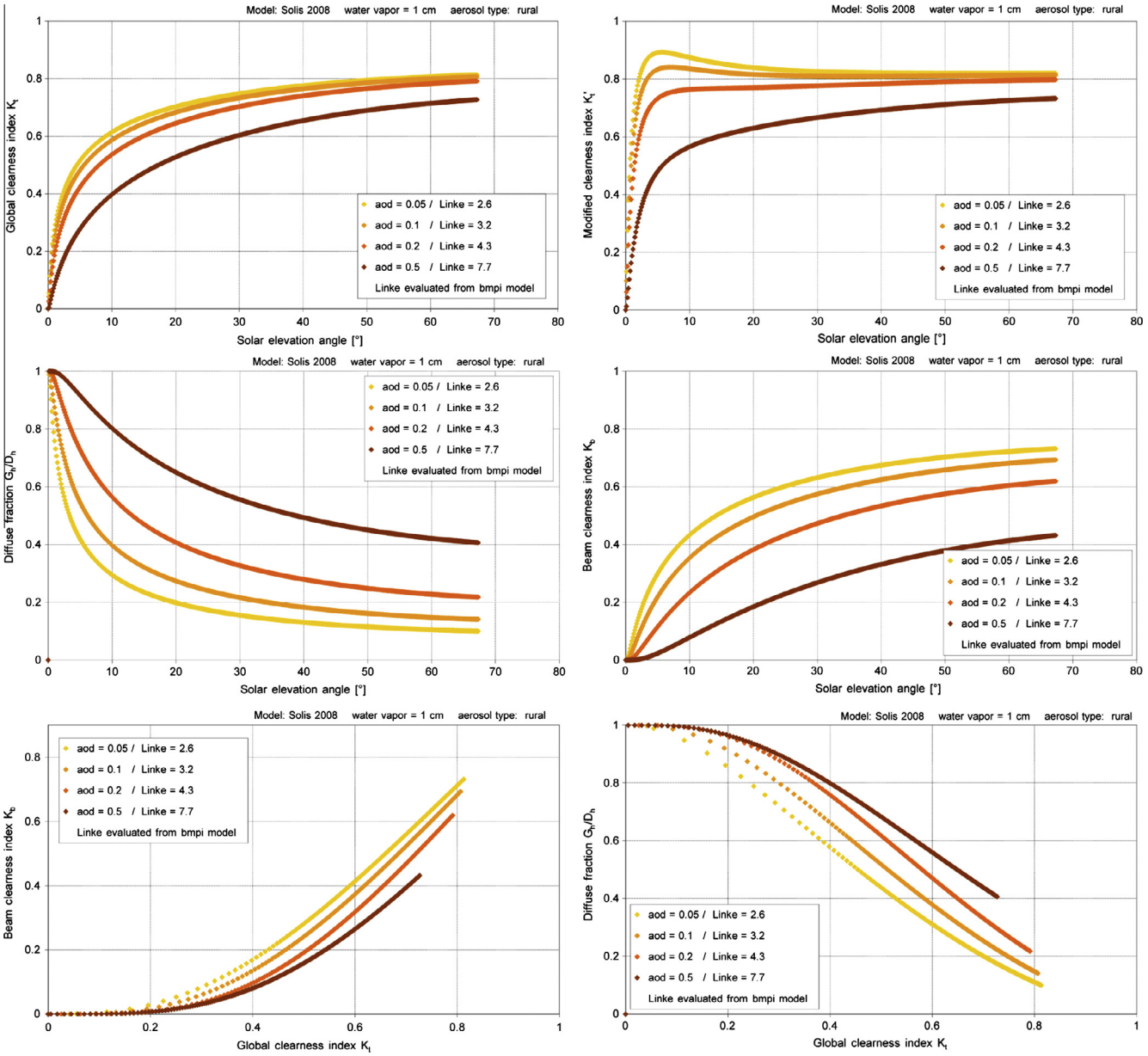

Fig. 3. Trends for the clearness indices and the diffuse fraction against the solar elevation angle and the global clearness index for the Solis model with rural aerosol type, 1 cm water vapor column and four values of aerosol optical depths.

cos z), the modified global clearness index K_t' (Perez, 1990), the beam clearness index K_b ($K_b = DNI/I_o$) and the diffuse fraction *DIF*/*GHI* (or D_h/G_h) are represented versus the solar elevation angle. The coherence of the components is illustrated by representing the diffuse fraction or the beam clearness index versus the global clearness index.

Fig. 4 is similar to Fig. 3, but focuses on small inconsistencies noted for each model for some of the considered relationship:

- *McClear (top left):* because of the reliance of LUT in the derivation of the clear sky radiation, the behavior of the global clearness index trend exhibits a discontinuous derivative for low elevation angles.
- *CPCR2 (top right):* for low values of the solar elevation angle, the derivative of the global clearness index shows a smooth inversion.
- *REST2 (center left):* for low solar elevation angles the global clearness index becomes incoherent. This effect is more pronounced for high aerosol load.
- *Bird (center right):* The distorted diffuse fraction shows that the consistency between the global and the beam components is not verified for global clearness indices lower than 0.4 and low aerosol optical depths.
- *Esra (bottom left):* the lowest possible global clearness index is 0.4 whereby the derivative exhibits an inversion.
- *Kasten:* The behavior is similar to the Bird model, but it is more pronounced.

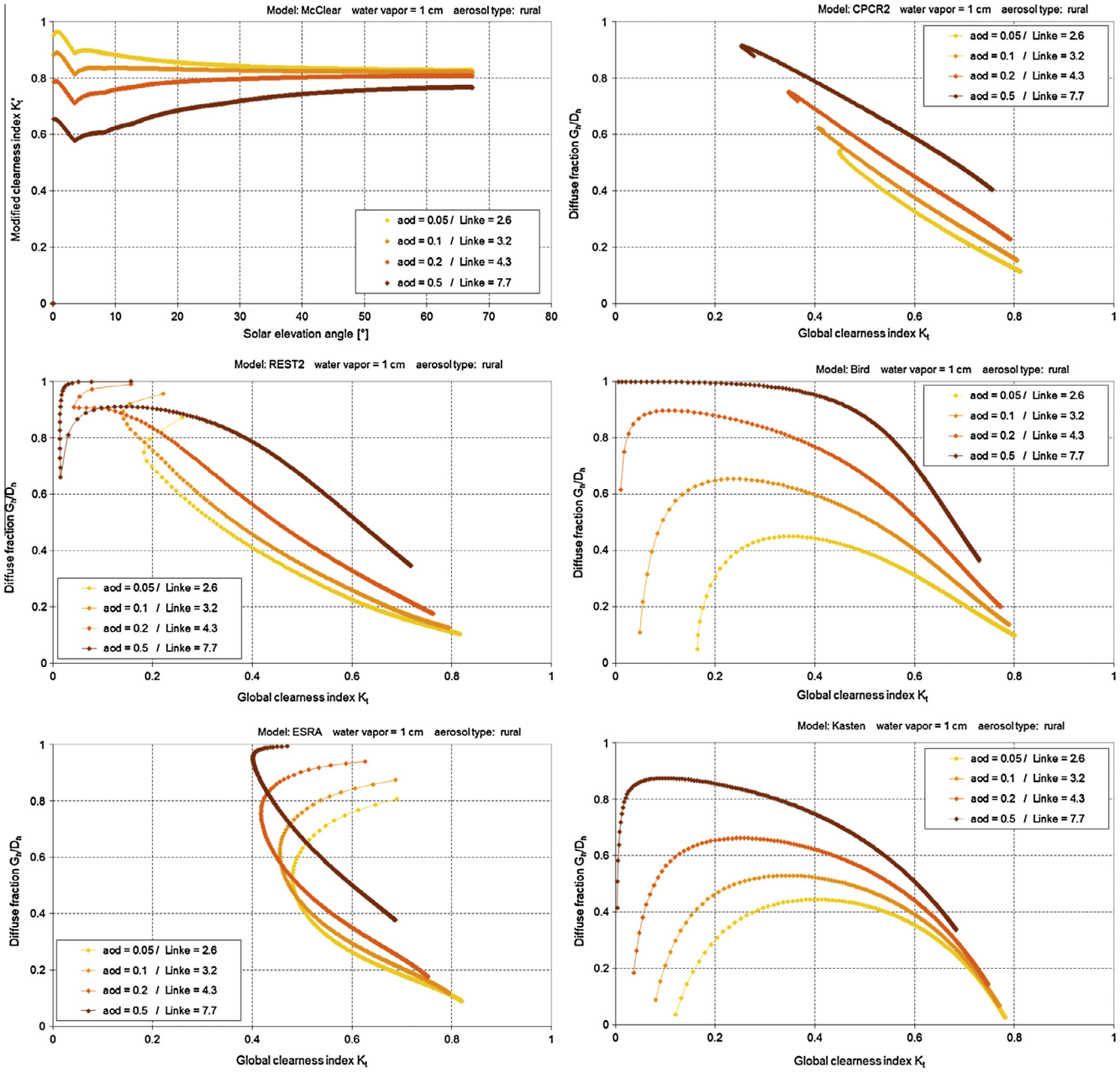

Fig. 4. Illustration of specific patterns for all the models (for Solis see Fig. 3).

- *Solis:* is the only model that shows no inconsistency in any of the trends (see Fig. 3).

These effects occur mainly at low solar elevation angles and the consequences on the overall model precision is only minor. On the other hand, for some models, the consistency between the global and the beam components is not verified for low values of K_t (lower than 0.4 for the ESRA model).

6. Model validation

The first step in the validation process is to compare selected measured data under clear sky conditions with modeled data. The validation is then quantified using classical first order statistical indicators: the mean bias difference (*mbd*) and the standard deviation (*sd*). Finally, the results are presented graphically for selected and representative sites and radiation components.

6.1. Clear conditions selection

To perform the selection, the following criteria are applied:

- The closure equation is the equation connecting together the three solar irradiance components: ($G_h = D_h + B_h$); it must be satisfied within -50 W/m^2 -5% and $+50$ W/m^2 $+5\%$,

Table 2
Statistics (*mbd*, *sd* and bias standard deviation *bsd*) for all the sites, models and 2 aerosol sources. The best ranked results are shaded.

Model	nb of clear sky hourly values	GHI (W/m^2)	Aerosol source: MACC			Aerosol source: bmpi			DNI (W/m^2)	Aerosol source: MACC			Aerosol source: bmpi		
			mbd (%)	sd (%)	bsd (%)	mbd (%)	sd (%)	bsd (%)		mbd (%)	sd (%)	bsd (%)	mbd (%)	sd (%)	bsd (%)
McClear	31,824	629	2.9	3.1	3.4	4.4	2.5	4.6	823	−0.7	6.5	4.1	2.2	3.6	4.4
REST2	33,334	632	−4.5	4.3	5.4	0.5	2.6	1.3	825	−15.8	8.3	16.6	0.3	3.4	2.8
CPCR2	33,799	635	0.6	3.0	3.0	3.5	2.7	3.7	825	−16.7	8.1	17.6	−0.1	3.3	2.6
Solis 2008	33,134	633	−0.2	3.4	2.8	2.9	2.4	3.2	825	−16.4	9.0	17.5	0.8	3.4	3.0
Bird	33,146	633	3.0	3.4	4.2	6.4	3.4	6.6	825	−10.9	8.1	12.0	5.5	4.4	6.2
ESRA	34,062	634	−7.1	5.7	8.1	0.8	3.4	1.9	824	−15.7	8.8	16.6	1.8	3.4	4.1
Kasten	33,146	633	−0.8	3.6	2.7	2.8	2.8	3.4	825	−14.5	7.9	15.3	0.5	3.8	3.1

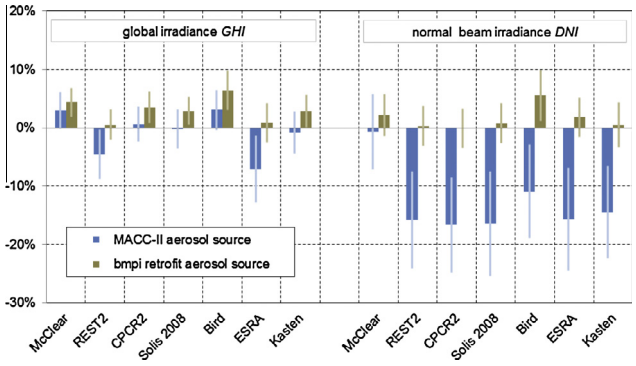

Fig. 5. Statistical results for the 2 components and all models, % of average irradiance, *mbd* (bars) surrounded by ± one standard deviation (lines).

- The global clearness index K_t of the measurements is lower than 0.82,
- the modified global clearness K_t' (Perez, 1990) of the measurements is higher than 0.65,
- the stability of the global clearness index $\Delta K_t'$ is better than 0.01 ($\Delta K_t'$ is evaluated by difference of the considered hour and the average of the considered hour, the preceding and the following hour),
- The broadband aerosol optical depth is lower than 0.5.

This selection is restrictive, but it ensures that only clear and stable conditions are selected. This is particularly important for high latitude sites where the conditions are often cloudy, and where a less restrictive selection can lead to erroneous statistical results biased by a few non-representative outliers. The number of hourly values selected through this procedure is given in Table 3 (see Section 7).

6.2. Statistical indicators and graphical representation

The comparison is done on an hourly basis, the model – measurements difference is computed, so that a positive value of the mean bias difference represents an overestimation of the model. The following indicators are used to quantify model performance:

- First order statistics for a given site: the mean bias difference (*mbd*) and the standard deviation (*sd*). In addition qualitative visualization is made with the help of model vs. measure scatterplots,
- The standard deviation of the bias (*bsd*), expressing the capability of the model to present a minimum spatial dispersion of the bias for the considered region of validation,
- The seasonal dependence of the bias and its dependence on aerosol optical depth (*aod*),
- The frequency distribution of the model-measure differences and the corresponding cumulated frequencies.

7. Results

The overall first order statistics for all the sites are presented in Table 2 for two aerosol sources: MACC-II project and *bmpi* retrofit. The table reports the total number of clear sky hourly values included in the validation, the hourly average irradiance value, the mean bias difference, the standard deviation and the standard deviation of the biases for the *GHI* and the *DNI*. The best ranked results are shaded.

The mains results are the following:

- For the MACC-II aerosol source, the best results are produced by the Solis model for the global component and by McClear for the beam component,
- For the *bmpi* aerosol source, respectively REST2 and CPCR2 give the best statistics.

The McClear model was developed with MACC-II aerosol data as its input; it has to be noted that, when using MACC aerosol inputs, all the other models present a high negative bias and a high dispersion of the biases for the beam component. This expresses the fact that the MACC-II data presents some weaknesses in representing correctly the aerosol amount and/or the aerosol type. On the contrary, when using *bmpi* data as input, which are ground based measurements, the three REST2, CPCR2 and Solis give better results. Fig. 5 is an illustration of these results.

A deeper analysis of the results leads to the following general observations:

- when the measured and modeled values for the selected clear sky conditions are presented on the same graph, it can be seen for all models and all sites that for a given global clearness index, the highest beam measurements, and consequently also the lowest diffuse values, are never reached by the modeled values (see the green points on the graphs in Fig. 6).

This is illustrated for the site of Kishinev and the McClear model in Fig. 6 where the diffuse fraction is plotted against the global clearness index on the left graph, and the beam clearness index against the global clearness index on the right graph.

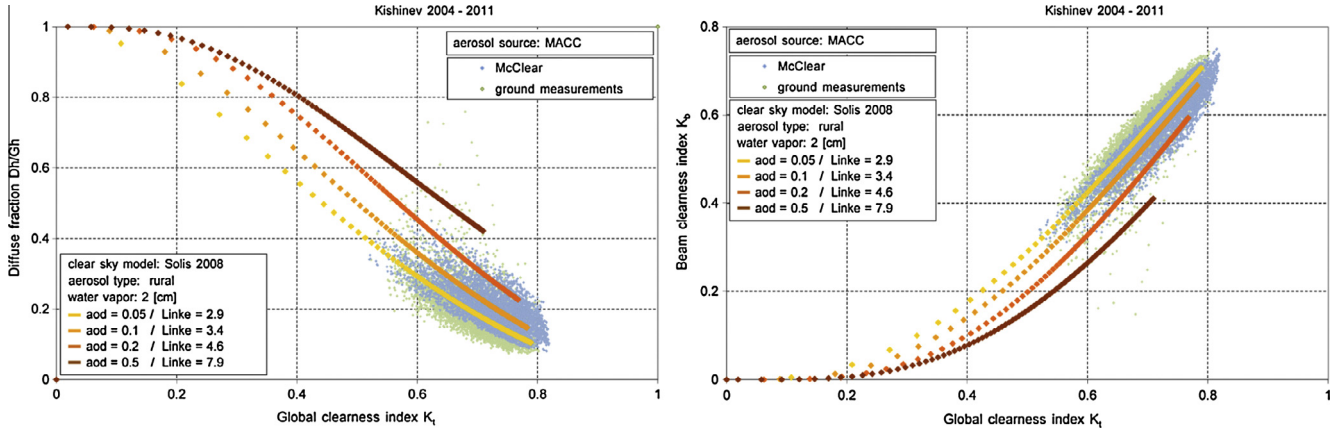

Fig. 6. Diffuse fraction (left) and beam clearness index (right) versus the global clearness index.

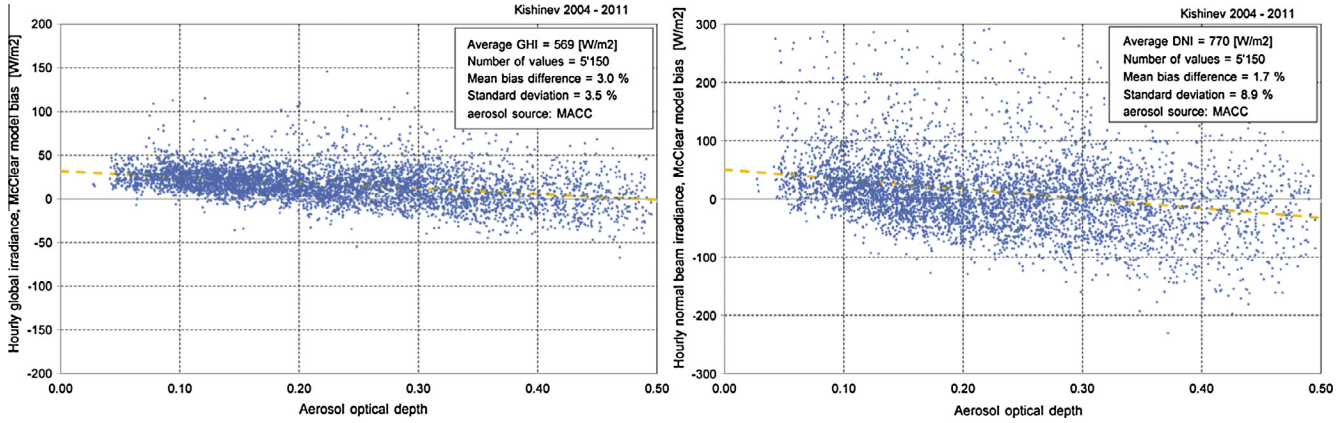

Fig. 7. Bias of the McClear model with MACC aerosol input versus the aerosol optical depth for GHI (left) and DNI (right), for the site of Kishinev.

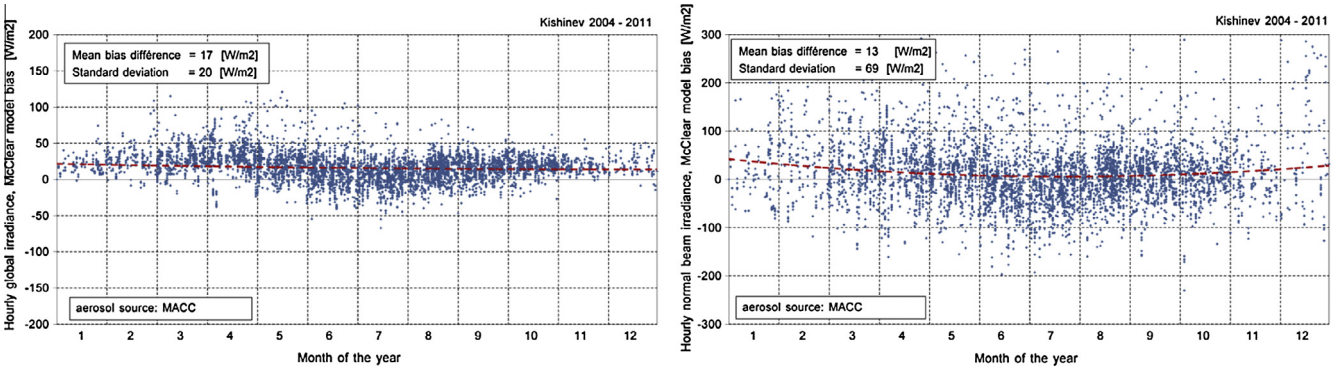

Fig. 8. Seasonal dependence of the bias for the global (left) and the beam (right) irradiance components for the site of Kishinev, the McClear model with MACC aerosol input.

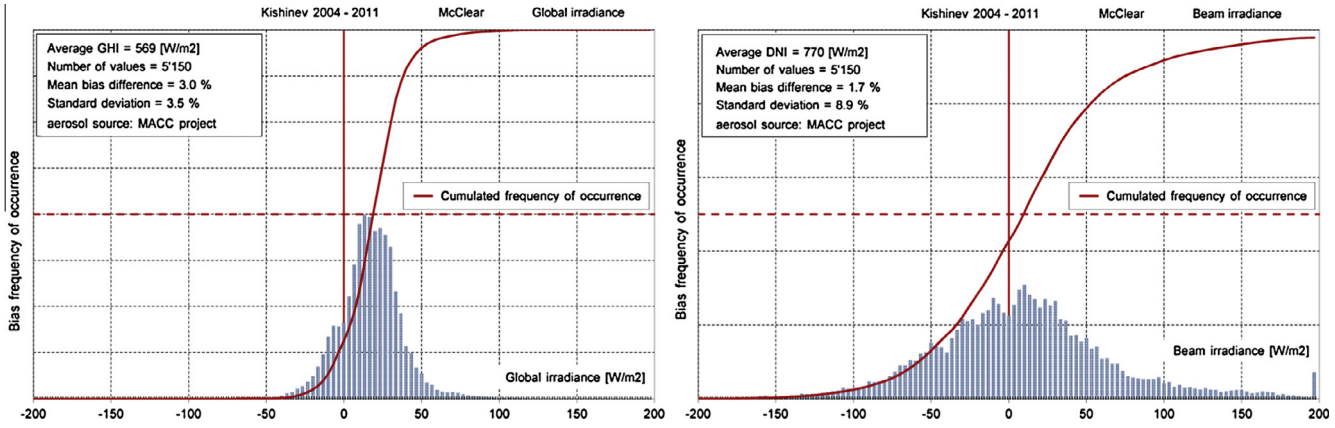

Fig. 9. Frequency of occurrence of the bias around the 1:1 axis for both components, for the site of Kishinev, the McClear model with MACC aerosol input.

The same pattern is visible regardless the *aod* values used as input to the models.

- The trend of the bias as a function of the aerosol optical depth exhibits a similar pattern for all the sites and models: when using MACC *aod* as input, the models' bias decreases with the optical depth for both the global and the beam components as illustrated in Fig. 7 for the site of Kishinev and the McClear model.

When the *bmpi* aerosol optical depth values are used, no specific pattern can be detected. It has to be noted that unlike the MACC values that are retrieved by a model, the *bmpi* values are retrieved from ground measurements; therefore, better results are expected for the latter input.

- The seasonal dependence of the bias for both the global and the beam irradiance components shows no specific pattern. It differs slightly from one site to the other regardless of the model and the aerosol input. An illustration is given on Fig. 8 for the site of Kishinev, for hourly values of the McClear model with MACC input.
- With the exception of a few specific sites like Davos or Mt Kenya, the distributions of the bias around the 1:1 model-measurements axis are near normal; for this reason the first order statistics represented by the mean bias and the standard deviation can be considered as reliable. An example is given in Fig. 9 for the site of Kishinev, with the McClear model with MACC input. The figure displays the hourly bias frequency distribution for both *GHI* and *DNI* irradiance components. The cumulated frequencies (red curve) are also represented.

To avoid displaying too many tables, detailed results are presented for only two models in Table 3. The table reports the number of hourly values used for the validation, the average measured irradiance, the absolute and relative mean bias difference, and the standard deviation. Results are provided for the three irradiance components and all sites. The overall statistics across all sites including the lowest and the highest mean bias, absolute bias, and standard deviation of the biases, are presented at the end of the table. The number of data from Mt Kenya is very low; therefore the site is not included in the overall results.

Table 3
Validation results for all the site, MacClear and Solis model, MACC and *bmpi* aerosol inputs. Mt-Kenya is not included in the overall statistics. The shaded values are the best (green) and the worst (orange) results.

Site	nb of hourly values	GHI					DNI					DIF				
		Average Wh/m^2 h	mbd		sd		Average Wh/m^2 h	mbd		sd		Average Wh/m^2 h	mbd		sd	
McClear model, hourly values – Aerosol source: MACC																
Almeria 2004–2011	4199	637	11	1.8%	15	2.4%	854	−24	−2.8%	47	5.6%	90	26	29%	24	27%
Bratislava 2004–2007	734	548	53	9.6%	23	4.3%	740	65	8.8%	63	8.5%	94	14	15%	23	25%
Cabauw 2005–2011	630	543	13	2.3%	17	3.2%	758	10	1.3%	56	7.4%	106	8	8%	25	24%
Carpentras 2004–2011	4686	587	14	2.5%	18	3.0%	820	−2	−0.2%	55	6.7%	85	19	23%	23	27%
Davos 2004–2011	700	657	−6	−1.0%	13	2.0%	954	−61	−6.4%	42	4.4%	59	38	64%	23	39%
Geneva 2004–2011	1899	622	42	6.7%	18	2.9%	814	29	3.6%	53	6.5%	83	24	28%	27	33%
Kassel 2004–2011	1465	585	12	2.0%	19	3.2%	793	4	0.5%	58	7.3%	87	24	28%	24	28%
Mt Kenya 2004–2007	12	377	0	0.0%	5	1.4%	834	3	0.4%	108	12.9%	71	−3	−5%	42	59%
Kishinev 2004–2011	1692	578	18	3.1%	16	2.8%	804	8	1.0%	45	5.6%	93	12	13%	18	19%
Lerwick 2004–2011	102	560	−9	−1.5%	13	2.3%	802	−44	−5.4%	55	6.8%	94	20	21%	25	26%
Lindenberg 2004–2011	500	509	4	0.8%	17	3.4%	782	−12	−1.5%	52	6.6%	86	11	13%	19	22%
Madrid 2004–2011	1485	618	26	4.2%	23	3.7%	858	11	1.3%	48	5.6%	73	27	38%	26	36%
Nantes 2004–2011	638	581	10	1.8%	19	3.2%	807	4	0.5%	56	6.9%	93	12	13%	26	28%
Payerne 2004–2011	1059	604	22	3.6%	17	2.8%	819	13	1.6%	60	7.3%	94	12	13%	24	26%
Sede Boqer 2004–2011	3718	744	11	1.5%	24	3.2%	868	−72	−8.3%	50	5.7%	101	65	64%	28	27%
Skukuza 2004–2007	1835	631	28	4.5%	26	4.1%										
Tamanrasset 2004–2011	2823	672	16	2.4%	17	2.5%	850	20	2.4%	62	7.3%	112	12	11%	32	29%
Toravere 2004–2011	984	500	12	2.4%	14	2.9%	806	−9	−1.1%	50	6.2%	75	19	25%	17	23%
Valentia 2004–2011	324	618	12	2.0%	23	3.6%	855	−56	−6.6%	54	6.3%	79	45	57%	23	29%
Vaulx 2004–2011	1240	651	34	5.3%	25	3.8%	817	25	3.1%	61	7.5%	92	24	26%	28	30%
Wien 2004–2011	837	603	31	5.1%	25	4.1%	767	36	4.7%	63	8.2%	109	9	8%	31	28%
Zilani 2004–2009	354	598	16	2.7%	25	4.1%	834	10	1.2%	47	5.6%	84	15	18%	19	23%
All sites	31,916	624	18	2.9%	20	3.1%	830	−6	−0.7%	54	6.5%	91	25	28%	25	28%
Lowest bias/sd			4	0.8%	13	2%		−2	−0.2%	42	4%		8	7.6%	17	19%
highest bias/sd			53	9.6%	26	4%		−72	8.8%	63	9%		65	64.3%	32	39%
Mean absolute bias			19	3.0%				25	3.0%				25	27.8%		
Bias standard deviation			21	3.4%				34	4.1%				30	33.1%		
Solis 2008 model, hourly values – Aerosol source: bmpi																
Almeria 2004–2011	4290	639	18	2.9%	16	2.5%	850	6	0.8%	27	3.2%	92	15	16%	17	19%
Bratislava 2004–2007	795	554	50	9.0%	19	3.4%	734	−8	−1.1%	30	4.1%	99	52	53%	19	20%
Cabauw 2005–2013	652	544	8	1.4%	8	1.5%	753	−6	−0.8%	30	4.0%	108	12	11%	11	11%
Carpentras 2004–2011	4729	588	15	2.6%	10	1.6%	819	−4	−0.5%	20	2.5%	86	20	23%	13	15%
Davos 2004–2011	700	657	5	0.8%	15	2.3%	954	6	0.6%	20	2.0%	59	6	11%	19	32%
Geneva 2004–2011	1920	623	34	5.5%	14	2.2%	813	2	0.2%	22	2.7%	84	34	40%	17	21%
Kassel 2004–2011	1492	586	12	2.1%	13	2.2%	791	−39	−4.9%	66	8.3%	88	50	57%	30	34%
Mt Kenya (2004–2007)	12	377	−3	−0.8%	14	3.8%	834	−61	−7.3%	83	9.9%	71	19	27%	30	42%
Kishinev 2004–2011	1847	582	21	3.6%	15	2.6%	798	−2	−0.2%	22	2.7%	97	20	21%	18	19%
Lerwick 2004–2011	102	560	−1	−0.1%	8	1.4%	802	1	0.1%	28	3.5%	94	4	5%	14	14%
Lindenberg 2004–2011	500	509	16	3.1%	8	1.7%	782	3	0.3%	22	2.8%	86	13	16%	9	10%
Madrid 2004–2011	1486	618	25	4.0%	18	2.9%	858	12	1.4%	30	3.4%	73	24	32%	20	28%
Nantes 2004–2011	649	583	9	1.5%	13	2.2%	806	−7	−0.9%	18	2.2%	94	14	15%	13	14%
Payerne 2004–2011	1065	604	17	2.8%	9	1.5%	818	7	0.9%	23	2.8%	94	9	9%	11	12%
Sede Boqer 2004–2011	4442	753	15	2.1%	19	2.5%	849	3	0.3%	19	2.2%	114	15	13%	12	11%
Skukuza 2004–2007	1829	645	5	0.7%	11	1.7%										
Tamanrasset 2004–2011	3222	687	20	2.9%	16	2.3%	834	71	8.5%	38	4.5%	124	−17	−13%	22	17%
Toravere 2004–2011	567	494	6	1.2%	11	2.2%	797	0	0.0%	18	2.2%	78	9	12%	13	17%
Valentia 2004–2011	332	616	12	1.9%	12	1.9%	848	3	0.4%	27	3.2%	82	10	12%	12	15%
Vaulx 2004–2011	1248	652	30	4.6%	23	3.5%	817	−4	−0.5%	19	2.3%	93	36	39%	21	22%
Wien 2004–2011	879	605	31	5.2%	19	3.1%	763	−6	−0.7%	22	2.9%	111	36	32%	21	19%
Zilani 2004–2009	376	600	9	1.5%	22	3.6%	825	−1	−0.1%	25	3.0%	89	16	18%	15	17%
All sites	33,134	633	18	2.9%	15	2.4%	825	6	0.8%	28	3.4%	96	18	18%	17	18%
Lowest bias/sd			−1	−0.1%	8	1%		0	0.0%	18	2%		4	4.6%	9	10%
Highest bias/sd			50	9.0%	23	4%		71	8.5%	66	8%		52	57.0%	30	34%
Mean absolute bias			18	2.9%				13	1.6%				21	21.9%		
Bias standard deviation			20	3.2%				25	3.0%				24	24.8%		

Because of the retrieval methodology, unlike the *bmpi* aerosol optical depths, the MACC aerosol data can be evaluated for any sky conditions. Therefore, the number of selected hourly values is twice higher for MACC than for *bmpi* input. In order to have comparable results, the statistics are given for all the models based on the same set of data. Nevertheless, the statistics obtained for the McClear model applied on the complete set of data are comparable.

8. Conclusions

A long term validation of seven hourly clear sky models has been conducted with benchmarking data from 22 sites across Europe and around the Mediterranean region. Validation data cover over up to eight years. Two sources of aerosol optical depth input data were used: Aeronet and MACC-II. The main results of this investigation are the following:

- The Solis model is the only model that shows coherent relationships between irradiance components for the complete range of solar elevation angles;
- The distributions of the model-measurements bias can be considered as normal distributions. Therefore first order benchmarking statistics such as mean bias error and standard deviation can be considered as reliable metrics.
- Three models exhibit roughly the same level performance and stand above the other models. These models are: McClear, REST2 and Solis. The standard deviations for these models are of the order of ±3% for the global component and ±4% to ±5% for the beam component. The standard deviations of the bias are also respectively ±3% and ±4% to ±6%. Considering that the measurements uncertainties are respectively around ±4% and ±3% for the global and the beam components, the validation results show that roughly all the models stay within this value for the global component whatever the aerosol input data set is, but none for the beam component with MACC aerosol input. When using *bmpi* aerosol input, the standard deviations of all the models stay around the measurements uncertainty.
- For a given global clearness index, none of the models can reproduce the highest measured direct irradiance values. The probable reason of this systematic underestimation at high global clearness indices could be the use of daily atmospheric aerosol load as input to the models to estimate hourly irradiance values. This is observed for all locations.
- The bias dependence upon aerosol optical depth shows the same pattern for all models and locations.
- No specific model seasonal dependence was observed.

Acknowledgments

The project is supported by the Swiss Federal Office of Energy (http://www.bfe.admin.ch/index.html?lang=en) under contract N° 500184-03.

The ground data are kindly provided by the Plataforma Solar de Almeria (PSA, DLR Spain), the Baseline Surface Radiation Network (BSRN), the Aerosol Robotic Network (Aeronet), the Global Aerosol Watch project (GAW), the CIE International Daylight Measurements Program (Commission internationale de l'éclairage IDMP), the Universidad Politecnica de Madrid (UMP, Spain), the Ecole Nationale des Travaux Publiques (ENTPE) in Lyon (France), the Centre Scientifique et Technique du Bâtiment (CSTB) in Nantes (France), the Institut für Schnee- und Lawinenforschung (SLF) and the Physikalisch-Meteorologisches Observatorium Davos (PMOD/WRC) in Switzerland, the Frauenhofer Institute für Winderergie und Energisystemtechnik in Kassel (IWES, Germany), and the Natural Resources and the Environment, Global Change and Ecosystem Dynamics Research Group (CSIR) in South Africa. Thank you to Richard Perez for his thorough rereading of the manuscript.

References

Aeronet, 2015. Aerosol Robotic Network Available from http://aeronet.gsfc.nasa.gov/ (last access in August 2015).

Atwater, M.A., Ball, J.T., 1976. Comparison of radiation computations using observed and estimated precipitable water. Appl. Meteorol. 15, 1319–1320.

Berk A, Bernstein LS, Robertson DC, 1996. ûMODTRAN: a moderate resolution model for LOWTRAN 7ý, GL-TR-89-0122 (1989), updated and commercialized by Ontar Corporation, 9 Village Way, North Andover, Mass. 01845.

Bird, R.E., Hulstrom, R.L., 1980. Direct insolation models. Trans. ASME J. Sol. Energy Eng. 103, 182–192.

Blanc, P., Gschwind, B., Lefèvre, M., Wald, L., 2011. The HelioClim project: surface solar irrradiance data for climate applications. Rem. Sens. 3. http://dx.doi.org/10.3390/RS3020343, 343-361.

BSRN, 2015. Baseline surface radiation network Available from: http://www.bsrn.awi.de/ (last access in August 2015).

Cebecauer, T., Suri, M., Gueymard, C., 2011. Uncertainty sources in satellite-derived Direct Normal Irradiance: How can prediction accuracy be improved globally? Proceedings of the SolarPACES Conference, Granada, Spain, 20–23 Sept.

Cutforth, H.W., Judiesh, D., 2007. Long-term changes to incoming solar energy on the Canadian Prairie. Agr. For. Met. 145, 167–175.

Engerer, N.A., Mills, F.P., 2014. KPV: a clear-sky index for photovoltaics. Sol. Energy 105, 679–693.

ESRA, 2000. In: Greif, J., Scharmer, K. (Eds.), Dogniaux, R., Page, J.K. (Scientific advisors), L. Wald, M. Albuisson, G. Czeplak, B. Bourges, R. Aguiar, H. Lund, A. Joukoff, U. Terzenbach, H. G. Beyer, E. P. Borisenko (Authors), European Solar Radiation Atlas, 2000, fourth ed. includ. CD-ROM. Published for the Commission of the European Communities by Presses de l'Ecole, Ecole des Mines de Paris, France.

Geiger, M., Diabaté, L., Ménard, L., Wald, L., 2002. A web service for controlling the quality of measurements of global solar irradiation. Sol. Energy 73 (6), 475–480.

Gueymard, C., 1989. A two-band model for the calculation of clear sky solar irradiance, illuminance, and photosynthetically active radiation at the earth surface. Sol. Energy 43 (5), 253–265.

Gueymard, C., 2001. Parametrized transmittance model for direct beam and circumsolar spectral irradiance. Sol. Energy 71 (5), 325–346.

Gueymard, C., 2003. Direct solar transmittance and irradiance predictions with broadband models. Part 1: detailed theoretical performance assessment. Solar Energy 74, 355–379, Corrigendum. Sol. Energy 76, 513.

Gueymard, C., 2004. High performance model for clear sky irradiance and illuminance. In: ASES Conference.

Hammer, A., Lorenz, E., Kemper, A., Heinemann, D., Beyer, H.G., Schumann, K., Schwandt, M., 2009. Direct normal irradiance for CSP based on satellite images of Meteosat Second Generation. In: SolarPACES 2009, Berlin.

Hansen, C.W., Stein J.S., Ellis A., 2010. Statistical Criteria for Characterizing Irradiance Time Series. Sandia report SAND2010-7314.

Ineichen, P., Perez, R., 2002. A new airmass independent formulation for the linke turbidity coefficient. Sol. Energy 73 (3), 151–157.

Ineichen, P., 2006. Comparison of eight clear sky broadband models against 16 independent data banks. Sol. Energy 80, 468–478.

Ineichen, P., 2008a. A broadband simplified version of the Solis clear sky model. Sol. Energy 82, 768–772.

Ineichen, P., 2008b. A broadband simplified version of the Solis clear sky model. Excel tool. Available from: http://www.unige.ch/energie/fr/equipe/ineichen/solis-tool/ (last access in August 2015).

Ineichen, P., 2008c. Conversion function between the Linke turbidity and the atmospheric water vapor and aerosol content. Sol. Energy 82, 1095–1097.

Ineichen, P., 2014. Long term satellite global, beam and diffuse irradiance validation. Energy Procedia 48, 1586–1596.

Kaiser, J.W., Peuch, V.-H., Benedetti, A., Boucher, O., Engelen, R.J., Holzer-Popp, T., Morcrette, J.-J., Wooster, M.J., 2012. The MACC-II Management Board: The pre-operational GMES Atmospheric Service in MACC-II and its potential usage of Sentinel-3 observations, ESA Special Publication SP- 708. Proceedings of the 3rd MERIS/(A)ATSR and OCLI-SLSTR (Sentinel-3) Preparatory Workshop, held in ESA-ESRIN, Frascati, Italy, 15–19 October.

Kasten, F., 1980. A simple parametrization of the pyrheliometric formula for determining the linke turbidity factor. Meteorol. Rdsch. 33, 124–127.

Kasten, F., 1984. Parametriesierung der Globalstrahlung durch Bedekungsgrad und Trübungsfaktor. Annalen der Meteorologie Neue Folge 20, 49–50.

Kasten, F., 1996. The Linke turbidity factor based on improved values of the integral Rayleigh optical thickness. Sol. Energy 56 (3), 239–244.

Lefèvre, M. et al., 2013. McClear: a new model estimating downwelling solar radiation at ground level in clear-sky conditions. Atmos. Meas. Tech. 6, 2403–2418.

Linke, F., 1922. Transmissions-Koeffizient und Trübungsfaktor. Beitr. Phys. fr. Atmos. 10, 91–103.

Mayer, B., Kylling, A., 2005. Technical note: the libRadtran software package for radiative transfer calculations – description and examples of use. Atmos. Chem. Phys. 5, 1855–1877. http://dx.doi.org/10.5194/acp-5-1855-2005.

Mayer, B., Kylling, A., Emde, C., Buras, R., Hamann, U., 2010. LibRadtran: library for radiative transfer calculations, Edition 1.0 for libRadtran version 1.5-beta http://www.libradtran.org (last access in August 2015).

Meteonorm 6.1, 2009. Global Meteorological Database for Engineers, Planners and Education http://www.meteonorm.com (last access in August 2015).

Meyer, R., Hoyer, C., Schillings, C., Trieb, F., Diedrich, E., Schroedter, M., 2003. SOLEMI: a new satellite-based service for high-resolution and precision solar radiation data for Europe, Africa and Asia. ISES Solar World Congress 2003, June 14–19, Göteborg, Sweden.

Molineaux, B., Ineichen, P., O'Neill, N., 1998. Equivalence of pyrheliometric and monochromatic aerosol optical depths at a single key wavelength. Appl. Opt. 37 (30).

Mueller, R.W., Dagestad, K.F., Ineichen, P., Schroedter-Homscheidt, M., Cros, S., Dumortier, D., Kuhlemann, R., Olseth, J.A., Piernavieja, G., Reise, C., Wald, L., Heinemann, D., 2004. Rethinking satellite based solar irradiance modelling - The SOLIS clear-sky module. Rem. Sens. Environ. 91, 160–174.

Müller, R.W., Matsoukas, C., Gratzki, A., Behr, H.D., Hollmann, R., 2009. The cm-saf operational scheme for the satellite based retrieval of solar surface irradiance – a lut based eigenvector hybrid approach. Rem. Sens. Environ. 113 (5), 1012–1024. http://dx.doi.org/10.1016/j.rse.2009.01.012.

Pelland, S., Remund, J., Kleissl, J., Oozeki, T., De Brabandere, K., 2013. Photovoltaic and Solar Forecasting: State of the Art. IEA PVPS Task 14, Subtask 3.1, Report IEA-PVPS T14–01, ISBN 978-3-906042-13-8.

Perez, R., Ineichen, P., Seals, R., Zelenka, A., 1990. Making full use of the clearness index for parametrizing hourly insolation conditions. Sol. Energy 45 (2), 111–114.

Rigollier, C., Bauer, O., Wald, L., 2000. On the clear sky model of the ESRA – European Solar Radiation Atlas – with respect to the Heliosat method. Sol. Energy 68 (1), 33–48.

Shettle, E.P., 1989. Models of aerosols, clouds and precipitation for atmospheric propagation studies. AGARD Conference Proceedings, Copenhagen, Denmark, 9–13 October.

Smith, W.L., 1966. Note on the relationship between total precipitable water and surface dew point. J. Appl. Meteorol. 5.

Stanhill, G., CohenN, S., 2001. Global dimming: a review of the evidence for a widespread and significant reduction in global radiation with discussion of its probable causes and possible agricultural consequences. Agric. For. Meteorol. 107, 255–278.

Stoekli, R., 2013. The HelioMont Surface Solar Radiation Processing. Scientific Report, MeteoSwiss No. 93.

Suri, M., Hofierka, J., 2004. A New GIS-based solar radiation model and its application to photovoltaic assessments. Trans. GIS 8 (2), 175–190.

WMO, 2008. Guide to meteorological instruments and methods of observation see http://www.wmo.int/e-catalog/detail_fr.php?PUB_ID=509&SORT=N&q= (last access in August 2015).

Zarzalejo, L.F., Polo, Jesús., Martín, Luis, Ramírez, Lourdes, Espinar, Bella, 2009. A new statistical approach for deriving global solar radiation from satellite images. Sol. Energy 83 (4), 480–484.